Langmuir
Article
pubs.acs.org/Langmuir

Low-Density/High-Density Liquid Phase Transition for Model Globular Proteins

Patrick Grosfils[†,‡] and James F. Lutsko*[,‡]

[†]*Microgravity Research Center, Chimie Physique E.P. CP 165/62, Université Libre de Bruxelles, Av. F. D. Roosevelt 50, 1050 Brussels, Belgium, and* [‡]*Center for Nonlinear Phenomena and Complex Systems CP 231, Université Libre de Bruxelles, Blvd. du Triomphe, 1050 Brussels, Belgium*

Received November 27, 2009. Revised Manuscript Received February 11, 2010

The effect of molecule size (excluded volume) and the range of interaction on the surface tension, phase diagram, and nucleation properties of a model globular protein is investigated using a combination of Monte Carlo simulations and finite temperature classical density functional theory calculations. We use a parametrized potential that can vary smoothly from the standard Lennard-Jones interaction characteristic of simple fluids to the ten Wolde−Frenkel model for the effective interaction of globular proteins in solution. We find that the large excluded volume characteristic of large macromolecules such as proteins is the dominant effect in determining the liquid−vapor surface tension and nucleation properties. The variation of the range of the potential is important only in the case of small excluded volumes such as for simple fluids. The DFT calculations are then used to study the homogeneous nucleation of the high-density phase from the low-density phase including the nucleation barriers, nucleation pathways, and rate. It is found that the nucleation barriers are typically only a few k_BT and that the nucleation rates are substantially higher than would be predicted by classical nucleation theory.

Introduction

One of the most important problems in biophysics is the characterization of the structure of proteins. It is well known that the main impediment to the determination of protein structure is the difficulty with which good-quality protein crystals can be produced. This has led to a large body of work focused on understanding the details of protein nucleation. In recent years, it has become apparent as a result of simulation, theoretical, and experimental studies that nucleation in general and protein nucleation in particular are strongly affected by the presence of intermediate metastable states.[1−5] This raises the possibility that by understanding the mechanism by which intermediate states affect nucleation the quality of the final result can be better controlled.

The practical importance of investigating the role of intermediate metastable states lies in the fact that the effective interactions of proteins in solution depend on their environment. Protein molecules interact via Coulombic forces mediated by the ionic solution in which they are dissolved. The effective interaction between two protein molecules therefore depends on the properties of the solution, particularly the salt used to create the solution and its pH. This is the reason for the well-known fact that some salts are more effective than others in bringing about protein crystallization (the Hofmeister effect).[6] The detailed confirmation of the connection between the properties of the solution and the effective intraprotein interactions has come from both computer simulation[7,8] and from theoretical studies of the phase diagram of proteins in solution.[9] One goal of the present work is to investigate what aspect of the effective interactions is most relevant in controlling the nucleation of the metastable phase.

Assuming that the effects of the solvent can, to first approximation, be entirely accounted for by an effective interaction potential between protein molecules, the problem of protein nucleation can be viewed as analogous to the nucleation of a solid from a dilute gas. In this way, Wilson observed that favorable conditions for protein nucleation are correlated with the behavior of the osmotic virial coefficient.[10] Rosenbaum et al. showed that the phase diagram of a large class of globular proteins can be mapped onto that of simple liquids with an interaction potential that depends on the ionic strength of the solvent.[11,12] One particular characteristic of proteins is that these models involve a hard-core repulsion and an attractive tail with the range of the attraction being quite small compared to the size of the hard core. It is known that as the range of the attraction becomes smaller, the critical point of the liquid−vapor transition is suppressed relative to the triple point until for sufficiently short-ranged potentials the liquid−vapor transition becomes metastable with respect to the vapor−solid transition.[5] It is under this circumstance that the metastable liquid phase is thought to play an important role in protein nucleation.

Despite the abundance of evidence for the role of the intermediate state from both simulation and experiment, there is still no really convincing theoretical description based on first principles. Lutsko and Nicolis showed that transitions from the vapor to the metastable liquid to the solid were advantageous relative to the direct vapor−solid transition based on the bulk free-energy surface,[13] but

(1) Vekilov, P. G. *Cryst. Growth Des.* **2004**, *4*, 671.
(2) ten Wolde, P. R.; Frenkel, D. *Science* **1997**, *77*, 1975.
(3) Nicolis, G.; Nicolis, C. *Physica A* **2005**, *351*, 22.
(4) Shiryayev, A.; Gunton, J. D. *J. Chem. Phys.* **2004**, *120*, 8318.
(5) Lutsko, J. F.; Nicolis, G. *J. Chem. Phys.* **2005**, *122*, 244907.
(6) Zhang, Y.; Cremer, P. S. *Curr. Opin. Chem. Biol.* **2006**, *10*, 658–663.
(7) Lund, M.; Jungwirth, P.; Woodward, C. E. *Phys. Rev. Lett.* **2008**, *100*, 258105.
(8) Boroudjerdi, H.; Kim, Y.-W.; Naji, A.; Netz, R. R.; Schlagberger, X.; Serr, A. *Phys. Rep.* **2005**, *416*, 129–199.
(9) Shiryayev, A.; Pagan, D. L.; Gunton, J. D.; Rhen, D. S.; Saxena, A.; Lookman, T. *J. Chem. Phys.* **2005**, *122*, 234911.
(10) George, A.; Wilson, W. W. *Acta Crystallogr., Sect. D* **1994**, *50*, 361.
(11) Rosenbaum, D. F.; Zukoski, C. F. *J. Cryst. Growth* **1996**, *169*, 752.
(12) Rosenbaum, D. F.; Zamora, P. C.; Zukoski, C. F. *Phys. Rev. Lett.* **1996**, *76*, 150.
(13) Lutsko, J. F.; Nicolis, G. *Phys. Rev. Lett.* **2006**, *96*, 046102.

 DOI: 10.1021/la904487z

that work neglected the effects of interfaces and, in particular, surface tension. The goal of the present work is to take a step toward filling in this gap by characterizing the liquid−vapor interfacial surface tension and the liquid−vapor transition in a model globular protein consisting of molecules interacting with the ten Wolde−Frenkel potential.[2] However, because of the metastable nature of the transition, such a characterization based on simulation is difficult. We found it impossible to stabilize the liquid−vapor interface for the model protein because of the strong tendency toward crystallization. We have therefore had to use an indirect approach consisting of a combination of theory and simulation. First, the ten Wolde−Frenkel model potential for globular proteins is generalized so that it depends on three independent parameters that allow it to be deformed continuously from a Lennard-Jones potential (i.e., a simple fluid) to the hard-core + tail ten Wolde−Frenkel (tWF) potential. We have performed simulations covering part of the range from simple fluid to protein and compare these to density functional theory calculations to show that the DFT remains quantitatively accurate as the hard-core radius is increased from zero, in the LJ potential, to a typical value in the tWF potential and as the range of attraction decreases. Whereas simulation becomes infeasible when the range becomes too small, the calculations are easily performed and the preceding agreement gives some confidence in the result. The DFT is then used to calculate the nucleation barrier using recently developed energy-surface techniques. We find, somewhat surprisingly, that the increase in the hard-core radius is much more important than the decrease in the range of the potential and is mostly responsible for a dramatic drop in surface tension. This observation is particularly relevant in the case of proteins because the properties of the effective interaction can be varied by changing controllable parameters, such as the pH of the solution, so that a primary goal is to determine those conditions most favorable to homogeneous nucleation. Our results indicate that, as far as the low-density/high-density part of the transition is concerned, varying the range of the potential has little effect.

In the next section, our model potential is defined, the Monte Carlo simulations are described, and the DFT calculations are also sketched. In section III, we describe the comparison between theory and simulation as the potential is varied from Lennard-Jones toward the model protein interaction and show quantitative agreement between theory and simulation. We then present the DFT results for the surface tension and nucleation barrier and nucleation rate as calculated from DFT and compared to classical nucleation theory. The article concludes with a discussion of our results.

Theoretical Methods

Simulation. Because of the complexity of the constituent particles and the solvent-induced interaction, globular proteins are often modeled, to a first approximation, by an effective interaction potential. In their study of the phase behavior of globular proteins in solution, ten Wolde and Frenkel proposed the following effective potential[2]

$$V(r) = \frac{4\varepsilon}{\alpha^2}\left(\left(\frac{1}{\left(\frac{r}{\sigma}\right)^2 - 1}\right)^6 - \alpha\left(\frac{1}{\left(\frac{r}{\sigma}\right)^2 - 1}\right)^3\right) \qquad (1)$$

This is a Lennard-Jones potential modified to capture the essential features that characterize the interaction of proteins in solution. The potential includes a hard-sphere repulsion at $r = \sigma$

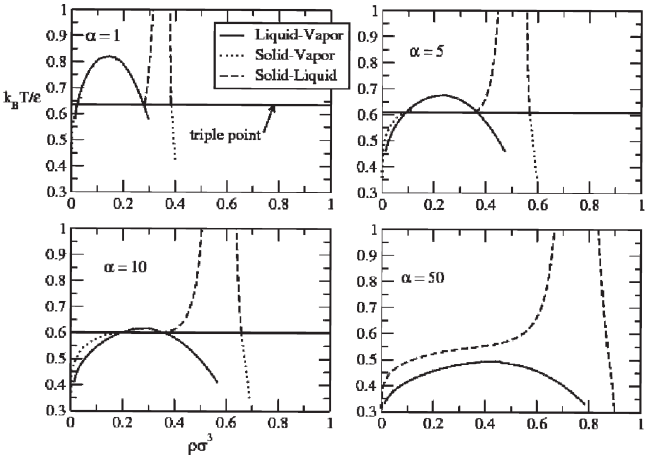

Figure 1. Calculated phase diagrams as a function of α for $\delta = 1$ showing that the liquid is metastable at $\alpha \geq 10$. From Lutsko and Nicolis.[5]

that accounts for the excluded volume (i.e., the size) of the protein molecule. Parameter α controls the range of solvent-induced effective attraction in that the minimum of the potential well occurs at $r = \sigma[1 + (2/\alpha)^{1/3}]^{1/2}$ whereas the minimum of the potential is $-\varepsilon$, independent of the value of the range. The range of the potential decreases when α increases, and for $\alpha = 50$, this model potential reproduces the phase behavior of globular protein solutions and, in particular, the well-known fact that for sufficiently short-range attractions the liquid phase becomes thermodynamically unstable,[2,5] as illustrated in Figure 1. For potential 1, this behavior is expected to be found when $\alpha \simeq 10$ in accordance with the generally accepted criteria according to which the range of the attraction should be ~25% of the range of the repulsive part to have a metastable liquid−gas coexistence.[5]

Metastable systems are notoriously difficult to study numerically because the liquid state spontaneously decays to the more stable crystal phase. In the present situation, the value $\alpha = 50$ puts the liquid−gas coexistence curve deep inside the unstable region, which makes the liquid phase difficult to maintain. A possible solution to this problem is to use constraints that restrict the configurational space of the system, thereby preventing the transition to the solid phase. There are different ways to constrain the system.[14] In the restricted Monte Carlo method,[15] the density is constrained to be below a limited value that thus suppresses the dense phase. Whereas this approach is well suited to the study of the supersaturated vapor phase, it is not appropriate for studying supercooled liquids because the densities of the liquid and solid phases are too similar. Another possibility would be to limit the number of neighbors per particle. This approach has been applied with success to a Lennard-Jones potential. However, there is a body of evidence that indicates that, besides its effect on the stability of liquids, the range of the attractive potential also impacts the structure of the liquid.[16] This fact could be of special importance in the present case because the structure of the liquid is atypical as a result of the large excluded volume that limits the number of interactions per particle. More generally, the shortcoming of restricted ensemble methods is the elimination of many configurations.

In this work, no constraints were imposed on the system. Stable liquid−gas equilibrium was obtained starting from a stable

(14) Nie, C.; Geng, J.; Marlow, W. H. *J. Chem. Phys.* **2007**, *127*, 154505.
(15) Corti, D. S.; Debenedetti, P. G. *Chem. Eng. Sci.* **1994**, *49*, 2717–2734.
(16) Doye, J. P. K.; Wales, D. J. *J. Phys. B* **1996**, *29*, 4859–4894.

two-phase state and modifying the temperature and parameter α step by step until the desired conditions were met. Unfortunately, for the desired case of $\alpha = 50$ this was not possible because there is no stable configuration from which to start. We therefore generalized the potential as

$$V(r) = \frac{4\varepsilon}{\alpha^2}\left(\left(\frac{1}{\left(\frac{r}{\sigma}\right)^2 - \delta^2}\right)^6 - \alpha\left(\frac{1}{\left(\frac{r}{\sigma}\right)^2 - \delta^2}\right)^3\right) \quad (2)$$

with a hard core at $r < \delta\sigma$ so that by varying dimensionless parameters α and δ it was possible to transition smoothly from a simple fluid, described by the Lennard-Jones interaction with $\alpha = 1$ and $\delta = 0$ and the model protein interaction with $\delta = 1$ and $\alpha = 50$. This allows a metastable liquid−gas coexistence to be reached from a stable Lennard-Jones system by varying the temperature and parameters α and δ in small steps.

We simulated an ensemble of $N = 1885$ particles interacting via potential 2 with a standard Metropolis Monte Carlo algorithm (MC-NVT).[17] The potential is truncated at $r_c = 2.8$ but not shifted. The particles are contained in a volume V with dimensions of $L_x = L_y = 9\sigma$ and $L_z = 108\sigma$, and periodic boundary conditions are imposed in all directions. To avoid the problem of stability of the liquid phase, the system is equilibrated during 5×10^5 Monte Carlo cycles (one cycle = N updates) at given (T, α, δ) starting from a stable initial configuration at $(T + \Delta T, \alpha + \Delta\alpha, \delta + \delta + \Delta\delta)$. The configuration of the system consists of a liquid slab of thickness $\Delta z \simeq 27\sigma$ surrounded along the z direction by two gas slabs. In this way, the stability of the liquid phase was maintained during the 10^6 cycles used to measure the density profile and the surface tension.

Surface tension can be measured by different methods. In a recent paper, we adopted the Bennett method, which appears to be precise.[18] However, we found it difficult to implement here for the following reason. In the Bennett method, the calculation of the surface tension follows from the definition

$$\gamma = \left(\frac{\partial F}{\partial A}\right)_{N,V,T} \quad (3)$$

where F is the free energy and $A = L_x \times L_y$ is the area of each liquid−vapor interface. In its implementation, the method requires one to compare the energies E_i $(i = 0, 1)$ of two configurations with different liquid−vapor interface areas A_0 and A_1. The configuration with interface area A_1 is obtained from the previous one by rescaling the positions of the particles:[17,19]

$$x' = x(A_1/A_0)^{1/2}$$

$$y' = y(A_1/A_0)^{1/2}$$

$$z' = z(A_0/A_1) \quad (4)$$

Because this perturbation is done at constant volume, the system is expanded along one direction and compressed along the transverse direction. Because of the isotropy of the fluid phase, this transformation has only a negligible effect on the energy of homogeneous systems because the energy change created by the displacement along the compression direction is compensated for by an energy change along the expansion direction. In the presence of an interface, the symmetry is lost and there is a net energy difference between the two configurations that is localized at the liquid−vapor interface. Although perturbation 4 is usually an efficient way to probe the interfacial free energy, we found it to be unsuitable here because the surface tension of the protein model is particularly small so that large perturbations are necessary to have a measurable free-energy difference. Unfortunately, large perturbations are inefficient when applied to systems whose potential contains an excluded volume because the compression step creates configurations with overlaps between particles. This not only gives infinite energy variation, but these variations are often located inside the liquid phase and not at the interface. To solve this problem, we implemented the interface wandering approach that allows a precise evaluation free-energy difference with small area perturbations.[20] In this method, the system is perturbed at each Monte Carlo cycle according to eq 4. Contrary to the Bennett method where the new configuration is only tested, in the interface wandering method the new area, chosen at random over the interval $[A_{\min}, A_{\max}]$, is effectively accepted with probability

$$P_{\text{accepted}} = \min(1, e^{-\beta(E_1 - E_0)}) \quad (5)$$

As a result of this acceptance ratio, the area of the interface evolves and is distributed between $A_{\min}$ and $A_{\max}$ according to a distribution f, which is related to the free energy

$$F = -k_B T \ln f \quad (6)$$

Because in this method many areas are sampled, instead of one in the Bennett method, curve fitting can be performed on the interface area distribution function, which allows a precise determination of the surface tension.

DFT Calculations. The properties of inhomogeneous systems were calculated using density functional theory. According to DFT, the free energy in the grand canonical ensemble, the grand potential Ω, is a functional of the local density, $\rho(\mathbf{r})$, and the applied external field, $\phi(\mathbf{r})$, of the form

$$\Omega[\rho] = F[\rho] + \int (\phi(\mathbf{r}) - \mu)\rho(\mathbf{r})\, d\mathbf{r} \quad (7)$$

where μ is the chemical potential, F and Ω both depend on temperature, and functional $F[\rho]$ does not depend on the field.[21,22] The equilibrium density distribution is determined by minimizing $\Omega[\rho]$. In a uniform system, the local density is a constant, where $\rho(\mathbf{r}) = \overline{\rho}$ and $F[\rho] \rightarrow F(\overline{\rho})$ is the Helmholtz free energy.

In our calculations, $F[\rho]$ is approximated using the modified-core van der Waals DFT model.[23] This is a generalization of the simplest hard-sphere plus mean-field tail model that gives quantitatively accurate descriptions of fluid structure,[23] surface tension,[18,23] and nucleation properties.[24] Here, we require quantitative accuracy in the DFT calculations because we wish to make

(17) Frenkel, D.; Smit, B. *Understanding Molecular Simulation*; Academic Press: Orlando, FL, 2001.
(18) Grosfils, P.; Lutsko, J. F. *J. Chem. Phys.* **2009**, *130*, 054703.
(19) Salomons, E.; Mareschal, M. *J. Phys.: Condens. Matter* **1991**, *3*, 3645–3661.
(20) MacDowell, L. G.; Bryk, P. *Phys. Rev. E* **2007**, *75*, 061609.
(21) Evans, R. *Adv. Phys.* **1979**, *28*, 143.
(22) Hansen, J.-P.; McDonald, I. *Theory of Simple Liquids*; Academic Press: San Diego, CA, 1986.
(23) Lutsko, J. F. *J. Chem. Phys.* **2008**, *128*, 184711.
(24) Lutsko, J. F. *J. Chem. Phys.* **2008**, *129*, 244501.

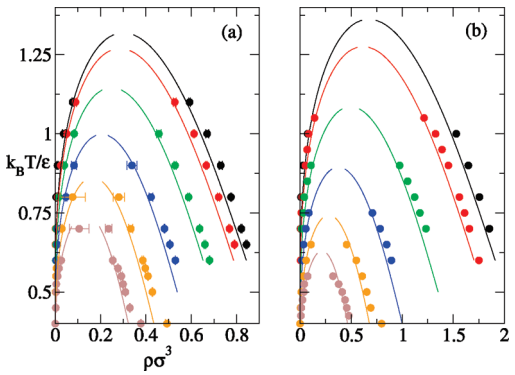

Figure 2. Phase diagrams for (a) $\alpha = 1$ and (b) $\alpha = 5$ as determined by simulation and theory for different values of the hard-core radius, $R = \delta\sigma$. The curves, from top to bottom, are for $\delta = 0$, 0.2, 0.4, 0.6, 0.8, and 1.0.

a direct comparison to simulation. In this model, the free energy is expressed as a sum of three contributions:

$$F[\rho] = F_{HS}([\rho]; d_{HS}) + F_{core}([\rho]; d_{HS}) + F_{tail}([\rho]; d_{HS}) \quad (8)$$

The first term on the right is the hard-sphere contribution, which is treated using the fundamental measure theory functional. The second term is the core correction, which is similar in form to the hard-sphere term but modifies the hard-sphere contribution so that the free energy in the bulk phase reproduces a given equation of state.[23] The last term is the tail contribution and has the simple mean-field form

$$F_{tail}([\rho]; d_{HS}) = \frac{1}{2}\int \Theta(r_{12} - d_{HS})\, \rho(\mathbf{r}_1)\, \rho(\mathbf{r}_2)\, v(r_{12})\, d\mathbf{r}_1\, d\mathbf{r}_2 \quad (9)$$

The reference hard-sphere diameter, d_{HS}, is calculated using the Barker−Henderson[22,25] expression

$$d_{HS} = \int_0^{r_0} (1 - e^{-\beta V(r)})\, dr \quad (10)$$

where r_0 is the distance at which the potential vanishes, $V(r_0) = 0$.

The model requires as input the bulk equation of state. For this, we use the Barker−Henderson first-order perturbation theory[22,25]

$$F(\bar{\rho}) = F_{HS}(\bar{\rho}; d_{HS}) + \frac{1}{2V}\bar{\rho}^2 \int \Theta(r_{12} - r_0)\, v(r_{12})\, g_{HS}(r_{12}; d_{HS})\, d\mathbf{r}_1\, d\mathbf{r}_2 \quad (11)$$

where $g_{HS}(r_{12}; d_{HS})$ is the hard-sphere pair distribution function in the fluid phase.

Results

Surface Tension. Figure 2 shows the phase diagrams obtained from the simulations as described above and as predicted using the thermodynamic perturbation theory for the cases of $\alpha = 1$ and 5. Away from the critical point, the agreement between theory and simulation is satisfactory over a wide range of hard-core radii. As is usual for a mean-field theory, the agreement near the critical point is not expected to be very good; therefore, this region has not been studied. The critical density and temperature for each system was estimated following the procedure in ref 18 and are given in Tables 1 and 2. The coexistence curves are shown in Figure 3 with the density and temperature scaled to the critical density and critical temperature, respectively. Although the generalized potential involves two length scales, σ controlling the position of the minimum and the hard-sphere radius $\delta\sigma$, the coexistence curves show typical corresponding states, as has been seen for other multilength scale potentials.[18]

A comparison between the surface tension as determined by simulation and from DFT calculations is shown in Figure 4. Increasing the size of the molecule (i.e., excluded volume parameter δ) at fixed α leads to lower surface tension: because the surface tension scales roughly with the critical temperature (Table 1), this trend is attributable to the decrease in critical temperature with increasing δ, which in turn is due to the increase of δ in the range of repulsion (which extends from $r = 0$ to $\delta\sigma + [\delta^2 + (2/\alpha)^{1/3}]^{1/2}$) compared to the range of the attractive part of the potential (and taking into account that the depth of the potential is fixed). However, for fixed δ, increasing α has little effect on $\delta = 1$ but leads to a significant increase in the surface tension for $\delta = 0$. In the latter case, the potential can be written as a function of single parameter $\sigma/\alpha^{1/6}$ so that one expects the

Table 1. Fits to Surface Tension $[\gamma(T) = \gamma_0 T_c(1 - (T/T_c))^{1.26}]$ for $\alpha = 1$[a]

d	T	γ_0	T_c (coex)	ρ_c (coex)
0.0	1.21	2.15	1.24	0.31
0.2	1.15	2.30	1.19	0.29
0.2	1.18	1.95	1.19	0.29
0.4	1.09	1.55	1.08	0.25
0.4	1.06	1.95	1.08	0.25
0.6	0.92	1.87	0.93	0.21
0.8	0.80	1.68	0.80	0.17
1.0	0.61	2.52	0.66	0.15

[a] The last two columns give the critical properties estimated from the coexistence data.

Table 2. Fits to Surface Tension $[\gamma(T) = \gamma_0 T_c(1 - (T/T_c))^{1.26}]$ for $\alpha = 5$[a]

d	T_c	γ_0	T_c (coex)	ρ_c (coex)
0.0	1.33	2.83	1.28	0.68
0.2	1.18	3.53	1.20	0.62
0.4	0.99	2.96	1.01	0.49
0.6	0.85	2.09	0.83	0.37
0.8	0.66	2.63	0.66	0.27
1.0	0.54	3.06	0.57	0.19

[a] The last two columns give the critical properties estimated from the coexistence data.

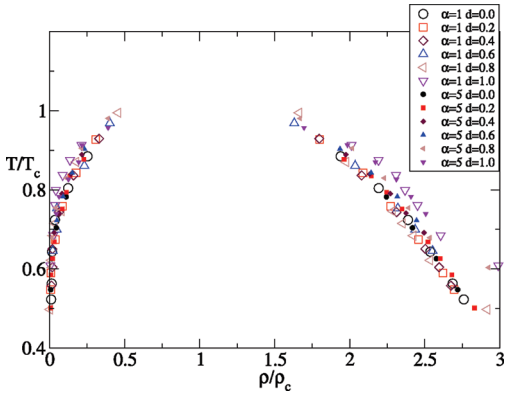

Figure 3. The same as Figure 2 with the density and temperature scaled to the critical density and temperature for each potential.

(25) Barker, J. A.; Henderson, D. *J. Chem. Phys.* **1967**, *47*, 4714.

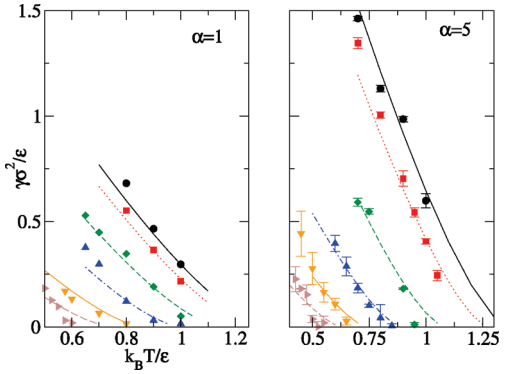

Figure 4. Surface tension as a function of temperature for (a) $\alpha = 1$ and (b) $\alpha = 5$ as determined by simulation and theory for different values of the hard-core radius, $R = \delta\sigma$. The curves, from top to bottom, are for $\delta = 0$, 0.2, 0.4, 0.6, 0.8, and 1.0.

surface tension in this case to vary as $\gamma \approx \alpha^{1/3}$. (Note that this scaling is somewhat spoiled by the fact that the cutoff used in the simulations was not scaled in the same way, so this should be taken only as an explanation of general trends.) In the former case of $\delta = 1$, the effect of changing α is mitigated by the relatively large (and fixed) effect of the excluded volume and, of course, the fixed depth of the potential minimum.

Because the surface tension goes to zero at the critical point and, as discussed above, the perturbative equation of state is least accurate near the critical point, it is not surprising that the relative accuracy of the theoretical calculations decreases as one approaches the critical point. Away from this region, however, the theoretical calculations are in good, nearly quantitative agreement with the simulations. On the basis of this comparison, the extension of the calculations to higher values of α seems justified.

Tables 1 and 2 also show the result of a fit to the expected form $\gamma = \gamma_0(1 - (T/T_c))^{1.26}$. Fitting both γ_0 and T_c and comparing to the critical temperature extracted from the coexistence data gives a consistency check for the analysis. In general, the temperatures derived by both methods are in reasonable agreement. The errors in the critical density are too large to permit us to make a definitive statement concerning whether the surface tension obeys the law of corresponding states.

Nucleation of Globular Proteins. Globular proteins are modeled using $\alpha = 50$ and $\delta = 1$ so that the liquid is metastable as shown in Figure 1. As discussed above, this makes simulation extremely difficult so that we present only the results of calculations using DFT. Indeed, the fact that the metastable phase immediately tends to nucleate the solid phase in simulation is one of the main reasons for focusing on the nucleation of the metastable phase because this appears to be the rate-limiting step. The agreement found above between DFT and simulation for lower values of α suggests that these results should be reasonable quantitative estimates. Figure 5 shows the surface tension as a function of temperature for different values of the hard-core radius. The trends noted earlier are repeated with the surface tension for $\delta = 0$ being approximately $50^{1/3} \approx 3.7$ times that for $\alpha = 1$ whereas the value of $\delta = 1$ is comparable to those for lower values of α.

The liquid−vapor transition is of particular interest because the metastable liquid phase is thought to play a key role in the process of precipitation of solid protein crystals from solution.[1,2,5] In classical nucleation theory (CNT), a liquid droplet is treated in the capillary approximation so that a droplet of radius R has excess free energy

$$\Delta\Omega = \frac{4\pi}{3}R^3(\omega(\rho_l) - \omega(\rho_v)) + 4\pi R^2\gamma \qquad (12)$$

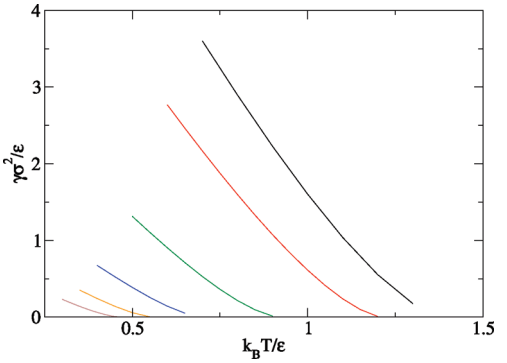

Figure 5. Surface tension as a function of temperature for $\alpha = 50$ as calculated using DFT. The curves, from top to bottom, are for $\delta = 0$, 0.2, 0.4, 0.6, 0.8, and 1.0.

where $\omega(\rho) = f(\rho) - \mu\rho$, $f(\rho)$ is the bulk Helmholtz free energy per unit volume of the fluid at density ρ, μ is the chemical potential, γ is the liquid−vapor surface tension at coexistence, and ρ_l and ρ_v are the densities of the coexisting liquid and vapor, respectively. In this model, the excess number of molecules in the droplet is

$$\Delta n = \frac{4\pi}{3}R^3(\rho_l - \rho_v) \qquad (13)$$

The free energy has a maximum at the critical radius, $R_c = 2\gamma/\Delta\omega$, with $\Delta\omega = \omega(\rho_v) - \omega(\rho_l)$, and a maximum, defining the barrier for nucleation, of $\Delta\Omega_{max} = 16\pi\gamma^3/3\Delta\omega^2$. Thus, from these simple considerations and the previously noted trends in the surface tension, we conclude that if all of the energy scales are proportional to T_c then the nucleation barrier will decrease with increasing molecular size (δ) and will vary weakly with the range of the potential, α.

To investigate the liquid−vapor transition in more detail, we have determined the nucleation pathway (specifically, the minimum free-energy path or MFEP) for the nucleation of liquid droplets from DFT to compare to the predictions of CNT for $T = 0.4\varepsilon$ or $T/T_c = 0.84$. The method of calculation is the same as described in detail in refs 24 and 26. The goal is to identify a path between the initial state (pure vapor) and the final state (pure liquid) that is minimal with respect to variations perpendicular to the path. (For a detailed explanation, see ref 27.) Figure 6 shows the free-energy barrier and the size of the critical cluster as a function of supersaturation, $S = (P_{coex} - P)/P_{coex}$, where the chemical potential at coexistence is $\beta\mu_{coex} = -2.354$ and the densities of the coexisting phases are $\rho_v = 0.109$ and $\rho_l = 0.626$. (Note that although the actual control variable in our calculations in the grand canonical ensemble is the chemical potential we use the more familiar definition of supersaturation in terms of pressure.) Figure 6 shows that classical nucleation theory is in agreement with DFT for small supersaturation but for large supersaturation the nucleation barrier calculated with DFT becomes very small, approaching zero as the vapor density approaches the spinodal, whereas CNT predicts a finite nucleation barrier at all densities. The Figure also shows that the excess number of molecules in the critical cluster is also well described by CNT except at large supersaturations. Figure 7, showing the critical clusters at different supersaturations, illustrates the reason for the failure of CNT at large supersaturation. It shows that large clusters are indeed well described by the capillary model, having very narrow interfaces. However, at large supersaturation, the

(26) Lutsko, J. F. *Europhys. Lett.* **2008**, *83*, 46007.
(27) Wales, D. *Energy Landscapes*; Cambridge University Press: Cambridge, U.K., 2003.

 DOI: 10.1021/la904487z E

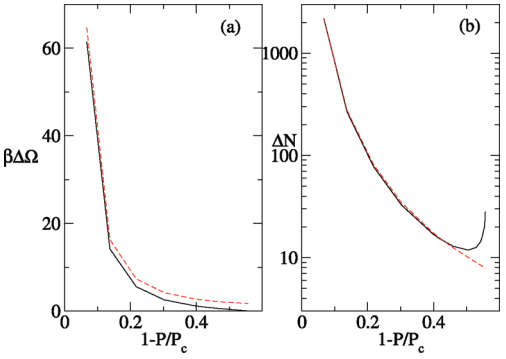

Figure 6. (a) Free-energy barrier for the nucleation of dense liquid from the low-density phase as a function of supersaturation. (b) Size of the critical cluster. In both cases, the solid lines are from the DFT calculations and the broken lines are from the prediction of CNT.

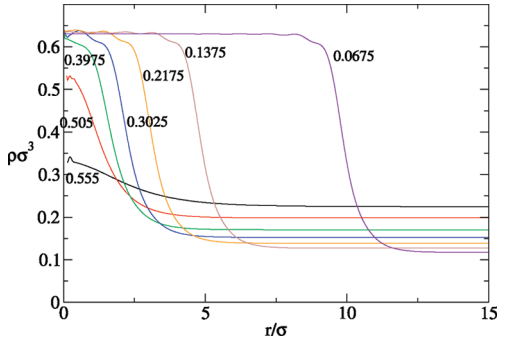

Figure 7. Density distribution in the critical clusters for various values of supersaturation.

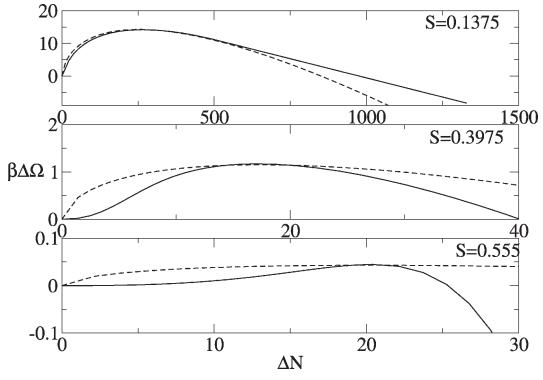

Figure 8. Excess free energy as a function of cluster size at three different values of supersaturation. The broken lines are a fit to CNT expression $\Delta\Omega = -(2\Delta\Omega/\Delta N_*)\Delta N + (3\Delta\Omega/\Delta N_*^{2/3})\Delta N^{2/3}$, where the starred quantities refer to the critical nucleus.

critical clusters are very small with most molecules affected by the interface and with central densities far below that of the bulk liquid. As a consequence, CNT fails to capture the very small barriers to nucleation. This final point is illustrated in Figure 8, which shows the nucleation pathway (i.e., the excess free energy as a function of cluster size) for three different supersaturations. At the smallest supersaturation, the barrier is well described by CNT. However, at large supersaturation, the shape of the nucleation barrier varies markedly from that assumed in CNT. In particular, there is virtually no free-energy penalty for the formation of small clusters.

Given that we have access to the nucleation pathway and not just the critical cluster, it is possible to evaluate the nucleation rate

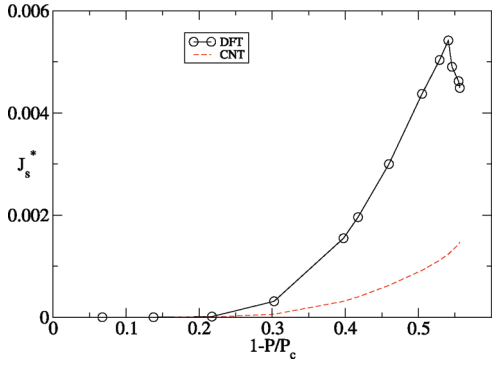

Figure 9. Dimensionless nucleation rate as a function of supersaturation. The scaled nucleation rate is $J_s^* = J\sigma^3/f_0$.

directly. Under the assumption of stationary nucleation and treating the number of molecules as a continuous variable, the nucleation rate is given by the otherwise exact expression

$$J_s = \left(\int_1^\infty \frac{dn}{f(n)\, C(n)} \right)^{-1} \tag{14}$$

where $f(n)$ is the monomer attachment rate for a cluster of size n and $C(n) = C_0 \exp(-\Omega(n)/k_BT)$ is the equilibrium distribution of cluster sizes.[28−30] The monomer attachment rate is assumed to be proportional to the surface area of a cluster and to the gas pressure, $f(n) = f_0(P/k_BT)n^{2/3}$ with $f_0 = \gamma c v_0^{2/3}(k_BT/2\pi m_0)^{1/2}$ where γ is the sticking probability for a monomer that collides with a cluster of size n (assumed here to be independent of n), c is a geometric factor, and m_0 and v_0 are the mass and volume of a molecule so that the area of the cluster is $cv_0^{2/3}n^{2/3}$.[30] Figure 9 shows the calculated nucleation rate as a function of supersaturation. The nucleation rate estimated from DFT is significantly higher than that estimated from CNT, in part because of the exponential amplification of the differences in barrier height seen in Figure 6 and in part because of the differences in the shape of the barrier.

Figures 6 and 9 both show nonmonotonic behavior near the spinodal. In the later case, the implication is that there is an optimal supersaturation that gives the maximal nucleation rate. However, this is likely to be an artifact of the calculations. As discussed in detail by Wilemski and Li,[31] mean-field models such as that used here and simpler models such as the square gradient model predict a divergent critical nucleus size at the spinodal due to the unrealistic mean-field equation of state. In any case, because the nucleation barrier is on the order of k_BT for $S \approx 0.4$, it is likely that the process of nucleation at higher supersaturations shares features of both nucleation and spinodal decomposition sometimes termed spinodal nucleation,[31,32] in which case the nucleation characteristics (rate and critical nucleus) would not be described by the simple theory given here. There are, therefore, two issues affecting the interpretation of these results. The first is the validity of mean-field theory, which definitely breaks down near the spinodal,[31,32] and the second is that even if the maximum occurred in the region of validity of the theory it would be masked by density fluctuations that would cause small volumes to become unstable with respect to spinodal decomposition.

(28) Zeldovich, J. B. *Zh. Eksper. Teor. Fiz.* **1942**, *12*, 525.
(29) Zeldovich, J. B. *Acta Physiochim. URRS* **1943**, *18*, 1.
(30) Kashchiev, D. *Nucleation: Basic Theory with Applications*; Butterworth-Heinemann: Oxford, U.K., 2000.
(31) Wilemski, G.; Li, J.-S. *J. Chem. Phys.* **2004**, *121*, 7821.
(32) Binder, K. *Phys. Rev. A* **1984**, *29*, 341.

Conclusions

In this article, we have constructed a pair potential that allows us to move smoothly from a simple fluid (i.e., Lennard-Jones interaction) to the short-ranged, hard Lennard-Jones used as a model for globular protein interactions. The potential depends on two parameters: the size of the molecule, characterized by the excluded volume parameter δ, and the range of the potential, controlled by the dimensionless parameter α. We compared the liquid−vapor surface tension as determined from Monte Carlo simulations to DFT calculations for the cases of $\alpha = 1$ and 5 and molecular radius ranging from zero to one (in Lennard-Jones units). Our results indicate that the combination of thermodynamic perturbation theory and the MC-VDW DFT model gives a good quantitative description of the liquid−vapor equation of state and surface tension over a wide range of temperature. Significant differences do appear as expected near the critical point because the mean-field equation of state is not accurate in this region. Our primary conclusion from these calculations is that it is the increase in excluded volume rather than the decrease in the range of the potential that causes a dramatic decrease in the surface tension. In fact, from Figures 4 and 5, one sees that whereas the surface tension for a zero hard-core radius is strongly affected by the range of the potential, the surface tension at the largest excluded volume is relatively insensitive to the range.

For fixed δ, changing α changes the range of the potential. However, the model potential can in fact be rewritten in terms of a single dimensioness parameter $\alpha\delta^6$ so that in absence of a cutoff, changing α and changing δ are in some sense equivalent. The actual physical relevance of the two parameters is that δ controls the size of the exluded volume and α controls the strength of the attractive interaction. Hence, one way to phrase our results is that changing the excluded volume has a much stronger effect on physical properties such as surface tension than does changing the strength of the attraction. These results suggest that increasing the excluded volume of a molecule leads to a decrease in surface tension and hence a decrease in the height of the barrier to the nucleation of the dense phase. Conformational changes can in fact be affected in some cases by changes in pH[33−35] and by light,[36] thus suggesting a means for taking advantage of this phenomenon to control crystallization rates in such systems.

For the $\alpha = 50$ case, we were not able to simulate the liquid−vapor interface because of the strong instability of the system to crystallization. Our theoretical calculations indicate similar behavior in the surface tension as found for smaller values of α. We have also calculated the nucleation pathway and thereby determined the barrier and rate of nucleation of liquid droplets from the vapor. We found very low barriers, less than $100k_BT$ even at relatively low supersaturation. Away from the spinodal, classical nucleation theory gives a good description of the barrier height and the size of the critical nucleus. At higher supersaturations, as the spinodal is approached, the nucleation pathway calculated from DFT differs significantly from that predicted by CNT. DFT also predicts a vanishing nucleation barrier at the spinodal and nonmonotonic behavior of the size of the critical nucleus and the nucleation rate near the spinodal. The shape of the barriers suggests that the excess free energy of small, subcritical clusters is very small, indicating that they might have relatively long lifetimes. However, the details of this picture become increasingly uncertain near the spinodal because of the limitations of mean-field theory and in any case may not be observable because they occur in the region of spinodal nucleation.

Acknowledgment. Our work has benefited from several discussions with Dominique Maes at the Flanders Interuniversity Institute for Biotechnology (VIB),Vrije Universiteit Brussel. This work was supported by the European Space Agency under contract number ESA AO-2004-070 and by projet ARCHIMEDES of the Communauté Française de Belgique (ARC 2004-09).

(33) Wang, Y.; Sha, M.; Ren, W. Y.; van Heerden, A.; Browning, K. S.; Goss, D. J. *Biochim. Biophys. Acta* **1996**, *1297*, 207–213.
(34) Wojtasek, H.; Leal, W. S. *J. Biol. Chem.* **1999**, *274*, 30950–30956.
(35) Lee, J. M.; Kay, C. M.; Watts, T. H. *Int. Immunol.* **1992**, *4*, 889–897.
(36) Rhinow, D.; Hampp, N. A. *J. Phys. Chem. B* **2008**, *112*, 13116–13120.